# CORRESPONDENCE OF THE PK VALUES OF OXYHB-TITRATION STATES DETECTED BY RESONANCE RAMAN SCATTERING TO KINETIC DATA OF LIGAND DISSOCIATION AND ASSOCIATION

R. SCHWEITZER-STENNER, D. WEDEKIND, AND W. DREYBRODT
*University of Bremen, Physics Department—FB 1, 2800 Bremen 33, Federal Republic of Germany*

ABSTRACT The dispersion of the depolarization ratio of oxidation and spinmarker lines of oxyhemoglobin at low $Cl^-$ concentration (<0.08 M) have been examined for different pH values in the acid and alkaline region. Interpreting the depolarization ratio dispersion curves by fifth order Loudon theory of the polarizibility tensor, we obtain tensor parameters depending linearly on symmetry classified distortions of the functional hemegroup. The pH dependence of these parameters are explained by assuming the influence of three titrable groups with $pK$ = 7.8, 6.6, and 5.8 on the heme. Using these $pK$ values, we are able to interpret the pH dependence of $CO(O_2)$-dissociation and CO-association of the fourth hemoglobin subunit. We conclude from our measurements that the change of the Tyr HC2$\beta$-configuration induces heme-apoprotein interaction via the Tyr HC2$\beta$-Val FG5$\beta$ H-bond, which are transduced to the heme via central and peripheral coupling.

## INTRODUCTION

Investigations of the heterotropic interactions between ligand-($O_2$, CO) and ion binding sites ($H^+$, $Cl^-$) in the hemoglobin system have been reported by an immense number of groups in the last twenty years. An unique and consistent interpretation of, for example, the alkaline and the acid Bohr effect, however, has not yet been given.

In terms of the two-state model of Monod et al. (1965), one assumes only pH variation of the R-T transition equilibrium constant $L$ to explain the Bohr effect. This is in accordance with x-ray studies of Perutz (1970), who obtained direct correlation between ligand binding, $pK$ shifts of amino acid residues (e.g., His HC3$\beta$, Val NA1 $\alpha$) and breaking of in subunit saltbridges that stabilize the hemoglobin $T$ structure.

On the other hand, much experimental data give clear evidence on a direct influence of $H^+$ binding on the tertiary structure of the protein subunits. Lindstrom and Ho (1973), measuring the NMR-Val E11 methyl resonances obtained a significant influence of the pD value on the Val E11-line-position. Several kinetic studies of Noble and co-workers (McDonald and Noble, 1972; De Young et al., 1976; Kwiatkowski and Noble, 1982*a, b, c*) have demonstrated that the dissociation rate of CO and $O_2$ ligands is reduced within the $R$ form of hemoglobin by increasing the pH from 6 to 9. Furthermore, Imai and Yonetani (1976) report that the hemoglobin $T$ state also exhibits a significant pH dependence. Consequently new allosteric models have been developed (Herzfeld and Stanley, 1974), which assumes $H^+$ to be a tertiary and quaternary effector. Yassin and File (1982) use the Herzfeld-Stanley model to analyze the pH dependence of human blood oxygen binding. From their data they deduce that $H^+$ ions directly influence the tertiary structure of the protein.

It is reasonable to assume that tertiary structure variations induced by $H^+$ binding influence the symmetry properties of the heme. As it has been shown by Schweitzer-Stenner et al. (1984*a, b*) and Schweitzer-Stenner and Dreybrodt (1985), the measurement of the depolarization (DRP) dispersion curves and the corresponding excitation profiles (EPs) of structural sensitive oxyHb Raman lines is a suitable tool to detect symmetry lowering distortions of the prosthetic porphyrin group induced by asymmetric side chains and different kinds of heme-apoprotein interactions (Mayer and Eicher, 1984). Using fifth-order time dependent perturbation theory (Loudon, 1973), the authors extract parameters by fitting simultaneously the experimental DPR-dispersion curves and excitation profiles. These parameters can be related to symmetry-classified normal distortions $\delta Q^\Gamma$ of the heme group ($\Gamma = A_{1g}$, $B_{1g}$, $B_{2g}$, and $A_{2g}$ representations in $D_{4h}$-symmetry).

Using this experimental and theoretical procedure, Schweitzer-Stenner et al. (1984*b*) show, that the $R$ state of oxyhemoglobin exhibits pH-dependent changes of tertiary structure at low and intermediate $Cl^-$ concentrations (0.1–0.3 M). Furthermore, Wedekind et al. (1985) measured DPR-dispersion curves and the corresponding (EPs)

Correspondence should be sent to Dr. Dreybrodt.

of structural sensitive oxyHb Raman lines at different $Cl^-$ concentrations and pH. Their results can be classified as follows: (*a*) at intermediate $Cl^-$ concentrations ($Cl^-$ = 0.1–0.3 M) both Raman lines investigated ($\Omega_R$ = 1,375 $cm^{-1}$ [oxidation marker], $\Omega_R$ = 1,638 $cm^{-1}$ [spin marker]) exhibit a strong variation of DPR dispersion in the region between pH 6.0 and 9.5. (*b*) at high $Cl^-$ concentration ($Cl^-$ = 1 M), the pH dependence of the oxidationmarker DPR dispersion is drastically reduced, whereas the spin-marker shows a strong pH dependence DPR-variation. (*c*) From the inspection of the normal mode pattern of the porphyrin system calculated by Abe et al. (1978) one can derive a different influence of peripheral and central heme apoprotein interactions on the properties of the investigated Raman lines as follows: central coupling via the $Fe^{2+}$-His F8 bond and His F8-porphyrin nitrogens (Warshel and Weiss, 1982) influences the DPR dispersion of the 1,375 $cm^{-1}$ oxidation-markerline (Ondrias et al., 1982), whereas the 1,638 $cm^{-1}$ spin-markerline reflects van der Waals interaction between the pyrrol side chains and the hydrophobic heme pocket. The different behavior of both Raman lines investigated at high $Cl^-$ concentrations can be explained in terms of these two coupling mechanisms.

To give an explanation for the influence of $Cl^-$ and $H^+$ ion binding on the heme properties as detected by resonance Raman scattering Wedekind et al. (1985) pointed out that their results are in accordance with Russu et al. (1980), postulating the existence of the functional important His HC3$\beta$-Asp FG1$\beta$ saltbridge in oxyHb at low $Cl^-$ and phosphate concentrations.

In this case the saltbridge must be assumed to be an important pathway of pH-induced structural variations of the $\beta$-subunit, where absence at high $Cl^-$ concentrations weakens the central coupling between the *F*-helix and the heme. This interpretation is in excellent agreement with measurements on oxyHb-BME (BME is bis(*N*-maleimidomethyl)ether) (c.f. Wedekind et al., 1985). In this system lacking the saltbridge between His HC3$\beta$ and Asp FG1$\beta$ (Simon, 1971) the pH dependence of both central and peripheral coupling is nearly absent. Other systems without this saltbridge (e.g., oxymyoglobin, deoxymyoglobin, methemoglobincyanide) also do not exhibit pH dependence of the oxidation marker DPR dispersion (el Naggar et al. 1985), thus supporting the model of Wedekind et al.

One has to take into account, however, that the interpretation of Russu's NMR data has recently been questioned by Perutz et al. (1985). These authors conclude from the comparison of NMR spectra of HbCO, Hb-Cowtown-CO (His HC3$\beta$-Leu) and other Hb mutants that the line assigned to His HC3$\beta$ by Russu et al. in reality is due to His FG4$\beta$, which titrates at $pK$ = 7.8 both in oxy and the deoxystate. They furthermore identified the line belonging to His HC3$\beta$ and found a $pK$ of 6.2 for this group in the absence of $Cl^-$ concentrations. From this they conclude that His HC3$\beta$ exhibits a $Cl^-$-dependent $pK$ shift (Kilmartin et al. 1973; Matsukawa et al., 1984), thus contributing to the alkaline Bohr effect also at low $Cl^-$ concentration (Kilmartin, 1980).

His FG4$\beta$ lies in a structurally sensitive part of the protein (Englander et al., 1983). In oxyHb-BME it is affected by the constraint induced by BME bridging covalently Cys F9$\beta$ and His FG4$\beta$. The new data reported by Perutz et al. are also in accordance with the Raman data of Wedekind et al. (1985). Therefore the reason for the *R*-state pH and $Cl^-$ dependence remains uncertain.

To obtain more insight on the influence of $H^+$ and $Cl^-$ binding, we have measured the DPR and EPs of the 1,375 and 1,638 $cm^{-1}$ Raman lines for different pH values at low $Cl^-$ concentrations (<0.08 M). Under these conditions $Cl^-$ binding can be excluded for oxyHbA (Rollema et al., 1975), and therefore a simple model can be derived (similar to those introduced by Schweitzer-Stenner et al. (1984*b*), which describes only the pH dependence of the polarizibility contributions of the different types of distortions $A_{1g}$, $B_{1g}$, $B_{2g}$, and $A_{2g}$ contributing to the Raman tensor reported in the first part of this paper.

In the second part we report on an interpretation of kinetic studies of $O_2$, CO dissociation, and association of the fourth hemoglobin subunit, also at low $Cl^-$ concentrations (De Young et al., 1976; Kwiatkowski and Noble, 1982*a*, *b*). They found that both dissociation and association constants of CO– and $O_2^-$ ligands exhibit a significant pH dependence. Therefore they conclude a pH dependence of the hemoglobin *R* state contrary to Imai and co-workers (Ikedo-Saito et al., 1977; Imai and Yonetani, 1976; Imai, 1981). Assuming that protonation of titrable amino acid groups causes this effect, we develop a simple model that enables us to obtain some understanding of the ligand binding procedure reflected by the kinetic measurements. From this we derive a formalism, by which the experimental data of ligand association (dissociation) can be fitted satisfactorily.

We have found that both sets of data, i.e., the pH dependence of the polarizibility tensor and the rate constants of ligand binding of the fourth subunit are related to the same set of $pK$ values ($pK$ = 7.8, 6.6, and 5.8). The most significant variation of ligand affinity and hemedistortion is caused by the protonation with $pK$ = 6.6.

The interpretation of kinetic association/dissociation measurements on des(His HC3$\beta$) and des(His HC3$\beta$, Tyr HC2$\beta$) lead to the conclusion that the H-bond between Tyr HC3$\beta$ and Val FG5$\beta$ is an important pathway of the tertiary structure variations induced by proton binding in the following sense: the protonation of surface histidines ($pK \approx 6.6$) (e.g., His HC3$\beta$) influences the equilibrium between two conformational states of the Tyr HC3$\beta$ aromatic ring (Shaanan, 1983; Johnson et al., 1978). This structural change is transduced to the heme via the H-bond between Tyr HC2$\beta$ and Val Fg5$\beta$ and the central and peripheral contacts between the heme and the F-, FG-helices of the protein.

In oxyHb-BME the "induced fit"-effect is blocked by

the constraint in the FG-helix, which is induced by BME bridging covalently Cys F9$\beta$ and His FG4$\beta$. Thus the pH dependence of heme apoprotein interaction is absent in agreement with the Raman data of Wedekind et al. (1985).

## THEORETICAL BACKGROUND

### Derivation of the Polarizibility Tensor

To describe the experimental results of the DPR and EP in oxyHb (Schweitzer-Stenner et al., 1984*a*, *b*) it was found to be necessary to extend the PNSF theory (Schweitzer-Stenner et al., 1984*a*, *b*), which is based on Loudon's formalism (Loudon, 1973) into fifth-order. This takes into account the vibrational sidebands of the *B*- and *Q*-band by creation and subsequent annihilation of vibrations giving rise to absorption in these bands. Symmetry perturbations from $D_{4h}$ are introduced into this formalism by expanding the vibronic coupling operators in the Hamiltonian with respect to equivalent normal distortions $\delta Q^{\Gamma_j}$. This leads to the expressions

$$\frac{\partial H}{\partial Q^{\Gamma_R}_{per}} = \frac{\partial H}{\partial Q^{\Gamma_R}}\bigg|_{\delta Q=0} + \sum_{\Gamma_j} \frac{\partial^2 H}{\partial Q^{\Gamma_R}\partial Q^{\Gamma_j}}\bigg|_{\delta Q=0} \cdot \delta Q^{\Gamma_j} \quad (1a)$$

$$\frac{\partial H}{\partial Q^{\Gamma_\mu}} = \frac{\partial H}{\partial Q^{\Gamma_\mu}}\bigg|_{\delta Q=0} + \sum_{\Gamma_j} \frac{\partial^2 H}{\partial Q^{\Gamma_\mu}\partial Q^{\Gamma_j}}\bigg|_{\delta Q=0} \cdot \delta Q^{\Gamma_j}. \quad (1b)$$

$\delta Q^{\Gamma_R}$ and $\delta Q^{\Gamma_\mu}$ relate to the normal coordinate of a Raman-vibration and the second phonon respectively. $\delta Q^{\Gamma_j}$ represents normal distortions of symmetry type $\Gamma_j$, which can be written as

$$\delta Q^{\Gamma_j} = \sum_i \delta Q_i^{\Gamma_j}, \quad (2)$$

where $\delta Q_i^{\Gamma_j}$ represents distortions proportional to the various different normal coordinates of the symmetry type $\Gamma_j$ ($A_{1g}$, $B_{1g}$, $A_{2g}$, and $B_{2g}$). Introducing this into the fifth-order expansion of the Raman tensor yields the perturbed tensor as

$$\begin{aligned}\beta_{\rho\sigma} = &\sum_{e,s=Q,B}\left[\mu_\rho^{ge}\mu_\sigma^{sg}\left(\sum_\Gamma C_{es}^{\Gamma,R}\,\hat{T}^\Gamma\right)\tilde{F}_{es}\right] \\ &+ \sum_{e,s,t,u=Q,B}\left\{\mu_\rho^{ge}\mu_\sigma^{sg}\times\left\{\left(\sum_\Gamma C_{es}^{\Gamma,R}\,\hat{T}^\Gamma\right)\right.\right. \\ &\cdot\left(\sum_\Gamma C_{st}^{\Gamma,\mu}\,\hat{T}^\Gamma\right)\left(\sum_\Gamma C_{tu}^{\Gamma,\mu}\,\hat{T}^\Gamma\right)F_1 \\ &+\left(\sum_\Gamma C_{es}^{\Gamma,\mu}\,\hat{T}^\Gamma\right)\left(\sum_\Gamma C_{st}^{\Gamma,R}\,\hat{T}^\Gamma\right)\left(\sum_\Gamma C_{tu}^{\Gamma,\mu}\,\hat{T}^\Gamma\right)F_2 \\ &+\left.\left.\left(\sum_\Gamma C_{es}^{\Gamma,\mu}\,\hat{T}^\Gamma\right)\left(\sum_\Gamma C_{st}^{\Gamma,\mu}\,\hat{T}^\Gamma\right)\left(\sum_\Gamma C_{tu}^{\Gamma,R}\,\hat{T}^\Gamma\right)F_3, \right.\right. \quad (3)\end{aligned}$$

where $\mu_\rho^{ge}$, $\mu_\sigma^{sg}$ are dipole transition matrix elements connecting the electronic groundstate and the excited electronic state $|e\rangle$, $|s\rangle$. ($\rho$, $\sigma = x, y, z$ label the polarization state of the transition).

The frequency functions $\tilde{F}$, $F_1$, $F_2$, and $F_3$ are defined by

$$\begin{aligned}\tilde{F} &= \{(\tilde{\nu}_e + \Omega_R - \tilde{\nu}_L + i\gamma^e)C\tilde{\nu}_s - \tilde{\nu}_L + i\gamma^s)\}^{-1} \\ F_1 &= \{(\tilde{\nu}_e + \Omega_R - \tilde{\nu}_L + i\gamma^e)(\tilde{\nu}_s - \tilde{\nu}_L + i\gamma^s)(\tilde{\nu}_t + \Omega_\mu - \tilde{\nu}_L + i\gamma^t) \\ &\quad\cdot(\tilde{\nu}_u - \tilde{\nu}_L + i\gamma^u)\}^{-1} \\ F_2 &= \{(\tilde{\nu}_e + \Omega_R - \tilde{\nu}_L + i\gamma^e)(\tilde{\nu}_s + \Omega_R + \Omega_\mu - \tilde{\nu}_L + i\gamma^s) \\ &\quad\cdot(\tilde{\nu}_t + \Omega_\mu - \tilde{\nu}_L + i\gamma^t)(\tilde{\nu}_u - \tilde{\nu}_L + i\gamma^u)\}^{-1} \\ F_3 &= \{(\tilde{\nu}_e + \Omega_R - \tilde{\nu}_L + i\gamma^e)(\tilde{\nu}_s + \Omega_R + \Omega_\mu - \tilde{\nu}_L + i\gamma^s) \\ &\quad\cdot(\tilde{\nu}_t + \Omega_R - \tilde{\nu}_L + i\gamma^t)(\tilde{\nu}_u - \tilde{\nu}_L + i\gamma^u)\}^{-1}. \quad (4)\end{aligned}$$

Antiresonant terms have been omitted for simplicity, $\tilde{\nu}_e$, $\tilde{\nu}_s$, $\tilde{\nu}_t$, $\tilde{\nu}_u$ are the wavenumbers of the electronic transitions from the groundstate $|g\rangle$ into $|e\rangle$, $|s\rangle$, $|t\rangle$, and $|u\rangle$ excited electronic states, which are indicating with the *Q* and *B* state of the porphyrin system, respectively, $\gamma^e$, $\gamma^s$, $\gamma^t$, and $\gamma^u$ label the corresponding halfwidths, $\tilde{\nu}_L$ is the frequency of the indicent laser light, $\Omega_R(\Omega_\mu)$ is the frequency of the Raman mode (the second phonon). The constants $C_{es}^{\Gamma_R}$, $C_{es}^{\Gamma_\mu}$ are related to the following matrix elements:

$$\begin{aligned}C_{e,s}^{\Gamma,R} &= \left\langle e\left|\frac{\partial H}{\partial Q^{\Gamma_R}}\right|_{\delta Q=0} + \frac{\partial^2 H}{\partial Q^{\Gamma_R}\partial Q^{\Gamma_j}}\bigg|_{\delta Q=0}\cdot\delta Q^{\Gamma_j}\right|s\right\rangle Q_R^{01} \\ C_{e,s}^{\Gamma,\mu} &= \left\langle e\left|\frac{\partial H}{\partial Q^{\Gamma_\mu}}\right|_{\delta Q=0} + \frac{\partial^2 H}{\partial Q^{\Gamma_\mu}\partial Q^{\Gamma_j}}\bigg|_{\delta Q=0}\cdot\delta Q^{\Gamma_j}\right|s\right\rangle Q_\mu^{01}. \quad (5)\end{aligned}$$

$Q_R^{01} = \langle 1|Q^{\Gamma_R}|0\rangle$ and $Q_\mu^{01}$ labels the vibronic matrix elements. $\Gamma_R(\Gamma_\mu)$, $\Gamma_j$ are the representations of the Raman mode (second phonon) and the normal distortions $\delta Q_j^\Gamma$ respectively, $\Gamma$, *R* labels the product representation $\Gamma_R \times \Gamma_j$ for each $\Gamma_j$.

Using the expression for $\beta_{\rho\sigma}$ and Placzek's (1934) formalism for calculating the EP and DPR from the Raman tensor components we are able to fit the theory to the experimental data, i.e. the DPR and EP with one common set of fit parameters $C_{e,s}^{\Gamma,R}$ and $C_{e,s}^{\Gamma,\mu}$ ($e, s = Q, B$; $\Gamma = A_{1g}$, $B_{1g}$, $A_{2g}$, and $B_{2g}$). These parameters $C_{e,s}^{\Gamma,R}$, $C_{e,s}^{\Gamma,\mu}$ are linearly related to the perturbations $\delta Q^{\Gamma_j}$ and their changes yield information on conformational changes of the Hb molecule. This procedure is described in detail elsewhere (Schweitzer-Stenner et al., 1984*a*, *b*).

### Calculation of Different Conformational Types

So far the theory is described assuming only one conformational type of Hb molecule to be present. In reality, due to various protonation processes, differing conformational states of the molecules, which are related to different polarizibility tensors, are present in the solution.

The different titration states $S_l$ present at a given pH value, can be characterized by the occupation numbers $\nu_i$

($\nu_i = 0,1$ labels the deprotonated, protonated state of an amino acid group $i$). At each pH value the complete polarizibility tensor $\beta^{\text{eff}}$ can be described as a superposition of tensors $\beta_l$, which are related to $S_l$. This leads to the following equation for the tensor components:

$$[\beta_{\rho\sigma}^{\text{eff}}]^2 = \sum_l \frac{n_l}{N} (\beta_{\rho\sigma})_l^2, \tag{6}$$

where $N$ is the total number of molecules.

The number $n_l$ of each kind of molecules can be calculated from mass action law as a function $n_l(K_1 \ldots K_i, \text{pH})$, where $K_i$ is the corresponding mass action constant of the $i$th group. Therefore, the fitting constants $C_{e,s}^{\Gamma,R}$, $C_{e,s}^{\Gamma,\mu}$ reflect effective scattering tensor contributions, which result from incoherent superposition of the Raman intensities due to each type of the molecule. From the fact that the EPs are only dependent on the squares of Placzek's tensor invariants (1934), one can conclude by some lengthly, but straight forward calculations that all $C_{e,s}^{\Gamma,R}$, $C_{e,s}^{\Gamma,\mu}$ exhibit a similar behavior as $\beta_{\rho\sigma}^{\text{eff}}$.

From this one obtains for $C_e^{\Gamma,R}$

$$\begin{aligned} C_{e,s}^{\Gamma,R} &= \left\{ \sum_l \frac{n_l}{N} [(\eta_{e,s}^{\Gamma,l}\, \delta Q_l^{\Gamma})]^2 \right. \\ &\quad \left. + (2\, \eta_{e,s}^{\Gamma,l}\, \epsilon_{e,s}^{\Gamma_R}\, \delta Q^{\Gamma_l}) + (\epsilon_{e,s}^{\Gamma_R})^2 \right\}^{1/2} \\ &\quad \Leftrightarrow \Gamma: = \Gamma_j \times \Gamma_R = \Gamma_R \\ C_{e,s}^{\Gamma,R} &= \left\{ \sum_l \frac{n_l}{N} [(\eta_{e,s}^{\Gamma,l}\, \delta Q^{\Gamma_h})^2] \right\}^{1/2} \\ &\quad \Leftrightarrow \Gamma: = \Gamma_j \times \Gamma_R \neq \Gamma_R, \end{aligned} \tag{7}$$

where

$$\begin{aligned} \eta_{e,s}^{\Gamma,l} &= \left\langle s \left| \frac{\partial^2 \mathrm{H}}{\partial Q^{\Gamma_R} \partial Q_l^{\Gamma_l}} \right| e \right\rangle Q_R^{01} \\ \epsilon_{e,s}^{\Gamma,R} &= \left\langle s \left| \frac{\partial \mathrm{H}}{\partial Q^{\Gamma_R}} \right| e \right\rangle Q_R^{01}. \end{aligned}$$

A similar equation can be derived for $C_{e,s}^{\Gamma,\mu}$.

For simplicity we summarize the fitting parameters due to one representation $\Gamma$ into one formalism as follows:

$$\begin{aligned} \sum_{A_{1g}}^{R} &= \left[ \sum_{e,s-Q,B} \left| C_{e,s}^{A_{1g},R} \right|^2 \right]^{1/2} \\ \sum_{B}^{R} &= \left[ \sum_{e,s-Q,B} \left( \left| C_{e,s}^{B_{1g},R} \right|^2 + \left| C_{e,s}^{B_{2g},R} \right|^2 \right) \Big/ 2 \right]^{1/2} \\ \sum_{A_{2g}}^{R} &= \left[ 2 \left| C_{QB}^{A_{2g},R} \right|^2 \right]^{1/2}. \end{aligned} \tag{8}$$

$\Sigma_{\Gamma'}^{R}$ ($\Gamma' = A_{1g}, B, A_{2g}$) labels the square root of the vibronic interaction strength induced by the distortions of the representation.

To explain the pH dependence of the $\Sigma_{\Gamma'}^{R}$ quantities obtained from our experiments we assume that three titratable groups influence the Raman scattering-tensor. From this we derive a model, which can be visualized by the diagram in Fig. 1 (Roux-Fromey, 1982).

The $C_{ijk}$ in Fig. 1 label different titration states of the molecule, the indices $i, j, k$ are due to the three different titrable groups, which are in the protonated ($i, j, k = 1$) or deprotonated state ($i, j, k = 0$) ($k, j, i$ are related to the equilibrium constants $K_1$, $K_2$, and $K_A$, respectively). The numbers $i, j, k$ are ordered with respect to rising $pK$ values. From the mass action laws one obtains

$$k_j = \frac{n_{i,j-1,k}\,[\mathrm{H}^+]}{n_{i,j-0,k}}. \tag{9}$$

The equilibrium constants $K_1$ and $K_2$ describe protonation in the physiological, the constant $K_A$ those in the acid region. The occupation numbers $n_{ijk}$ of the states $C_{ijk}$ can be calculated by the following equations:

$$\begin{aligned} \frac{n_{000}}{N} &= \left[ 1 + \frac{[\mathrm{H}^+]}{K_2} + \frac{[\mathrm{H}^+]}{K_1} + \frac{[\mathrm{H}^+]^2}{K_1 K_2} + \frac{[\mathrm{H}^+]^2}{K_1 K_A} \right. \\ &\quad \left. + \frac{[\mathrm{H}^+]}{K_A} + \frac{[\mathrm{H}^+]^2}{K_2 K_A} + \frac{[\mathrm{H}^+]^3}{K_1 K_2 K_A} \right]^{-1} \\ \frac{n_{001}}{N} &= \left[ 1 + \frac{K_1}{[\mathrm{H}^+]} + \frac{[\mathrm{H}^+]}{K_2} + \frac{K_1}{K_2} + \frac{[\mathrm{H}^+]}{K_A} \right. \\ &\quad \left. + \frac{[\mathrm{H}^+]^2}{K_2 K_A} + \frac{K_1}{K_A} + \frac{[\mathrm{H}^+] K_1}{K_2 K_A} \right]^{-1} \\ \frac{n_{010}}{N} &= \left[ 1 + \frac{[\mathrm{H}^+]}{K_1} + \frac{K_2}{[\mathrm{H}^+]} + \frac{K_2}{K_1} \right. \\ &\quad \left. + \frac{[\mathrm{H}^+] K_2}{K_1 K_A} + \frac{[\mathrm{H}^+]^2}{K_1 K_A} + \frac{K_2}{K_A} + \frac{[\mathrm{H}^+]}{K_A} \right]^{-1} \\ \frac{n_{011}}{N} &= [1 + K_1 K_2/[\mathrm{H}^+]^2 + K_1/[\mathrm{H}^+] \\ &\quad + K_2/[\mathrm{H}^+] + K_2/K_A \\ &\quad + [\mathrm{H}^+]/K_A + K_1 K_2/([\mathrm{H}^+] K_A) + K_1/K_A]^{-1} \end{aligned}$$

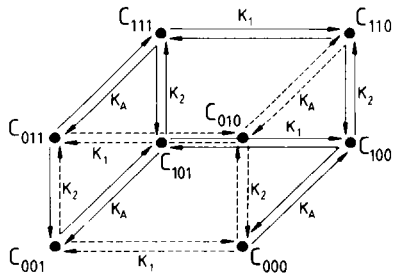


FIGURE 1 Equilibria between the different protonation states $C_{ijk}$, $i, j, k = 0$ or 1 when the corresponding groups are deprotonated or protonated. The equilibrium constants are denoted $K_1$, $K_2$, $K_A$.

$$\frac{n_{100}}{N} = [1 + [H^+]/K_2 + [H^+]/K_1 + [H^+]/(K_1K_2) + K_A/[H^+] + K_A/K_2 + K_A/K_1 + K_A[H^+]/(K_1K_2)]^{-1}$$

$$\frac{n_{110}}{N} = [1 + K_2K_A/([H^+])^2 + K_2K_A/(K_1[H^+]) + K_A/[H^+] + K_A/K_1 + [H^+]/K_1 + K_2/[H^+] + K_2/K_1]^{-1}$$

$$\frac{n_{101}}{N} = [1 + K_1/[H^+] + [H^+]/K_2 + K_1/K_2 + K_A/[H^+] + K_1K_A/(K_2[H^+]) + K_1K_A/[H^+]^2 + K_A/K_2]^{-1}$$

$$\frac{n_{111}}{N} = [1 + K_1K_2K_A/[H^+]^3 + K_1K_A/[H^+]^2 + K_2K_A/[H^+]^2 + K_A/[H^+] + K_2/[H^+] + K_1K_2/[H^+]^2 + K_1/[H^+]]^{-1}.$$

Inserting Eq. 9 into Eq. 7, we are able to fit the pH dependence of the Raman tensor parameters $\Sigma^R_{A_{1g}}$ and $\Sigma^R_B$. We use the $pK$ values $pK_1$, $pK_2$, $pK_A$ and the tensor parameter values $\Sigma^R_{\Gamma'}$ $(i, j, k)$ $(\Gamma' = A_{1g}, B)$ of the different titration states $C_{ijk}$ as fitting parameters.

It should be finally noted that for the interpretation of the pH dependence of some $\Sigma^R_{\Gamma'}$ quantities a further $pK$ value reflecting the influence of a basic residue ($pK = 9.0$) has been introduced. Since its protonation is of less importance for the region between pH 6.0 and 8.0 the corresponding titration states have been omitted in Fig. 1 and Eq. 9 for clarity.

## MATERIAL AND METHODS

### Material

Human adult hemoglobin was prepared from freshly drawn blood by standard procedure described by Schweitzer-Stenner et al. (1984*a*). To adjust the pH value, $HbO_2$ has been dialyzed against 400 ml 0.1 M bis-tris- and tris-buffer.

The concentration of $HbO_2$ ($\sim 10^{-3}$ M) has been determined by measuring the optical absorbance.

### Methods

The exciting radiation was obtained from an Argon-ion laser. The laser beam, polarized perpendicularly to the scattering plane, was focused by a cylindrical lens onto the sample, which was situated in a copper block for cooling to 6°C. A polarizer between sample and entrance slit of the Czerny Turner double monochromator enables us to measure the intensity of the two components polarized perpendicularly ($I_\perp$) and parallel ($I_\parallel$) to the scattering plane. To eliminate the different transmission of the spectrometer for the two components, a polarization scrambler was placed between polarizer and entrance slit.

To obtain the excitation profiles of the Raman lines we have taken into account the transmission dispersion of the polarizer and the spectrometer. The transmission of the polarizer has been measured with a Cary absorption spectrometer. The spectral response of the spectrometer system including the photomultiplier was determined by measuring the Raman intensity of several lines of calcite and quartz for each laserline of the $Ar^+$ laser, and correcting for the $\tilde{\nu}^4$ frequency dependence. This is possible since these materials have a frequency-independent Raman tensor. Since in our spectrometer we use a ruled grating, which does not show any anomalities in transmission, the spectral response of the spectrometer system can be obtained by interpolating between the measured points.

A correction for absorption of the samples is not necessary since absorption of the solution for the concentration of maximal $10^{-3}$ mol/monomer is of the order of 8 $cm^{-1}$. The length of the scattering volume, imaged to the entrance slit is ~100 $\mu$m, which is by a factor of 10 smaller than the penetration depth of the exciting radiation into the sample. All data given in Figs. 1–4 are calibrated to a heme concentration of $8 \cdot 10^{-4}$ M.

The collection cone of the backscattered radiation has an half-angle of 30°. According to the calculations of Deb et al. (1984) on the error in DPR due to finite collection angles this produces a maximal error of +6% from the real DPR value for lines with $\rho = 0.125$; for lines with $\rho = 0.75$ the maximal error is +1.7% and for $\rho = 2$ the maximal error is −6%. This error is almost exclusively from the $I_\parallel$ component of the radiation, whereas the error in the $I_\perp$ component is practically negligible. Since all these errors are in the range of our statistical errors, we have not corrected for them.

## RESULTS

Fig. 2 *a* shows the pH dependence of the oxidationmarker ($\Omega_R$ = 1,375 $cm^{-1}$) DPR dispersion and the corresponding EPs for pH values between pH 6.0 and 8.5 measured at $Cl^-$ concentrations lower than 0.08 M. In comparison to the corresponding curves at intermediate $Cl^-$ concentration (Schweitzer-Stenner et al., 1984*b*), one obtains a reduced minimum-maximum behavior and pH dependence of the DPR-dispersion curves. The spin marker (Fig. 2) exhibits similar behavior: between pH 6.9 and 7.8 only small variations of DPR-dispersion occur. In the acid and alkaline region, however, the DPR-dispersion curves vary their shape, indicating a change in heme symmetry perturbation.

Fig. 3 shows the pH dependence of the quantities $\Sigma^R_{A_{1g}}$, $\Sigma^R_B$ $\Sigma^R_{A_{2g}}$ defined in the theoretical section. The full lines result from a fitting procedure according to the preceding section. In the limit of accuracy, good agreement has been obtained. The $pK$ values of the three titratable groups assumed in our model are 7.8, 6.6, and 5.8 for each parameter $\Sigma^R_\Gamma$ of the oxidation-marker and spin-marker line, respectively. The $pK = 9$ has detectable influence only for pH >8 and is of minor importance in this context. Some comments should be given concerning the uniqueness of the fitting procedure due to the titration model visualized in Fig. 1. At first sight it seems to be quite dubious to use eleven free parameters to fit a set of six data points. Otherwise the following arguments have to be taken into account: (*a*) We are able to fit five independent sets of data using the same set of $pK$ values, i.e. $pK$ = 5.8, 6.6, and 7.8. (*b*) Most of the titration states visualized in Fig. 1 have very small occupation numbers. Therefore they do not contribute to Raman scattering. In the region between pH 6.0 and 8.0 only three states ($C_{000}$, $C_{001}$, $C_{011}$) are of

significant relevance for the scattering processes. Thus the number of fitting parameters is reduced from 11 to 6. Their values are tabulated in Table I.

Furthermore we have measured the pH dependence of $B$, $Q_v$, and $Q_o$-band extinction coefficient in the region between pH 4.0 and 9.0 at low $Cl^-$ concentrations. Fitting these experimental data using a similar titration model as introduced in the theoretical section of this paper, $pK$ values of 4.3, 5.3, 6.8, 7.8, and 9.0 have been obtained (Brunzel et al., 1986). This agrees satisfactorily with the data derived from Raman measurements.

From this we obtain confidence in the biophysical relevance of our results, i.e., the $pK$ values of those titrable groups influencing the symmetry properties of the heme.

## DISCUSSION

### Comparison of Raman Data with Kinetic Measurements

From the measurements and analyzation of pH-dependent DPR-dispersion curves of oxyhemoglobin Raman lines we have derived the influence of three (four) titrable amino acid groups on the symmetry properties of the functional hemegroup. To obtain more knowledge about the biophysical nature of these interactions we compare our results to other experimental data reflecting the pH dependence of the liganded $R$ state of Hb.

De Young et al. (1976) and Kwiatkowski and Noble (1982*a*, *b*) have reported kinetic measurements of the fourth subunit's ligand dissociation and association rate constants at low $Cl^-$ concentration. They have found a significant pH dependence of these rate constants in the region between 6.0 and 8.0. Fig. 4 shows the pH-induced variation of $O_2$-dissociation rate and CO-dissociation and association rate constants. The dissociation rate constant of both, CO and $O_2$, decreases from pH 6.0 to 8.0. The association constant of CO, however, is minimal at pH 6.0, and increases drastically toward pH 8.0. Thus, the ligand binding equilibrium, expressed by $K = l_4/l_4'$, shows a minimum in the acid and a minimum in the alkaline part of the physiological region (Fig. 5).

From this we assume that our titration model is also able to describe the kinetic results. To test this assumption, Eq. 9 has been introduced in the formalism describing the dissociation/association processes in the following way: Dissociation of a ligand $L$ of the fourth subunit is described

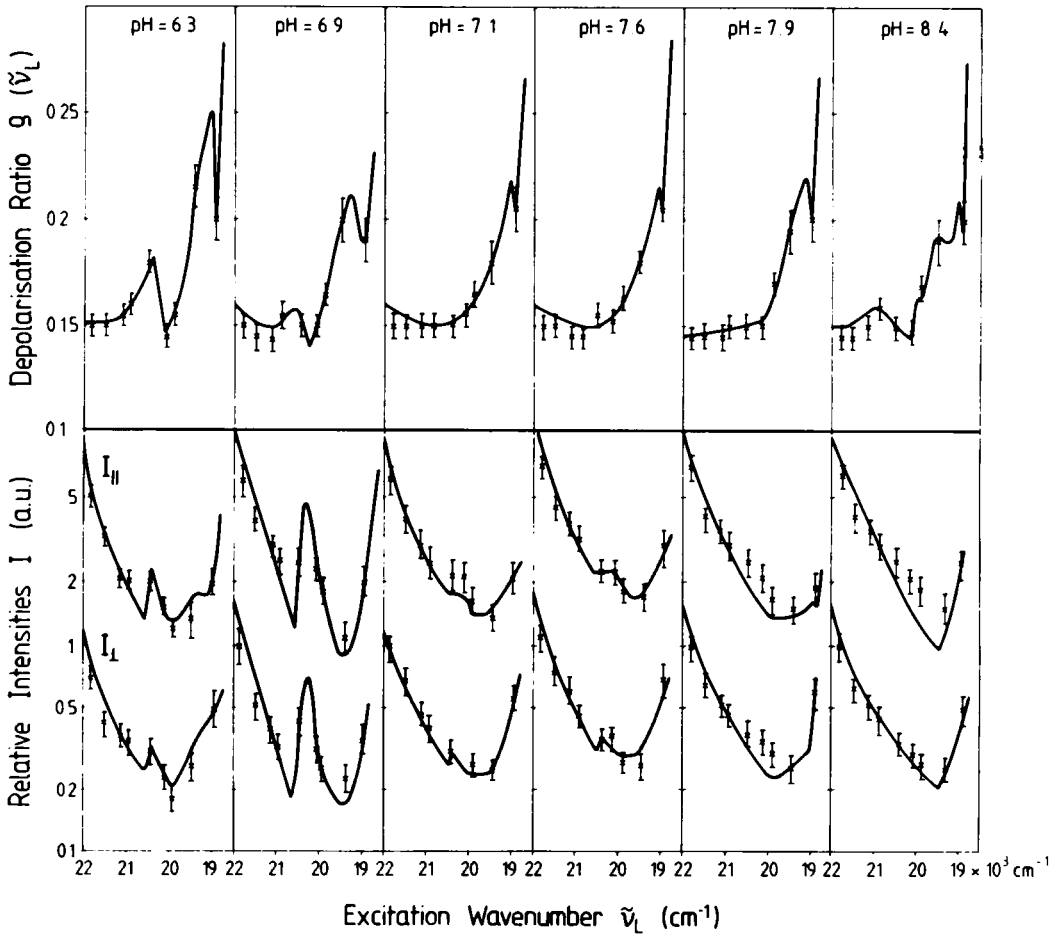


FIGURE 2 DPR dispersion curves and EPs of the 1,375 and 1,638 $cm^{-1}$ lines of oxyHb for different pH values at $[Cl^-] < 0.08$ M.

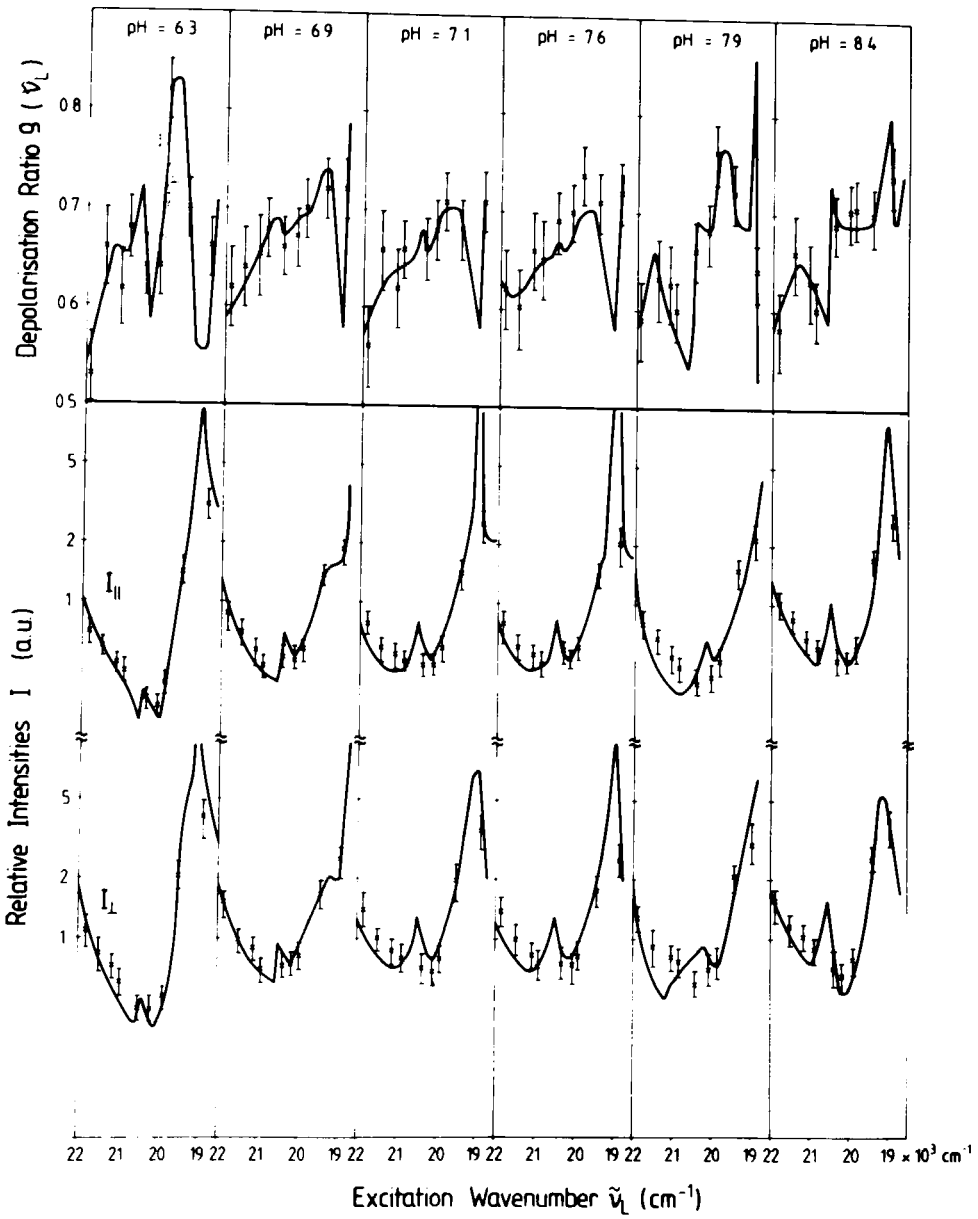


FIG. 2 con't.

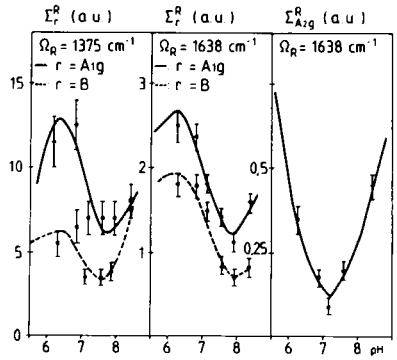


FIGURE 3 $\Sigma^R_{A_{1g}}$ (pH), $\Sigma^R_B$ (pH) diagrams of the 1,375 $cm^{-1}$- and 1,638 $cm^{-1}$-Raman line of the oxyHb spectrum for $[Cl^-]$ <0.08 M (the full lines are calculated by the fitting procedure).

TABLE I

| Titration state | $\Sigma^R_{A_{1g}}(C_{ijk})$ | $\Sigma^R_B(C_{ijk})$ |
|---|---|---|
| $C_{000}$* | 3.0 | 3.0 |
| $C_{001}$* | 5.43 | 3.00 |
| $C_{011}$* | 17.92 | 8.7 |
| $C_{000}$‡ | 0.5 | 0.5 |
| $C_{001}$‡ | 1.1 | 0.82 |
| $C_{011}$‡ | 3.7 | 2.73 |

Tensor parameters $\Sigma^R_{A_{1g}}(ijk)$, $\Sigma^R_B(ijk)$ of the different titration states $C_{ijk}$ at $[Cl^-]$ < 0.08 M calculated by the fitting procedure ($i, j, k = 0.1$).
*$\Omega_R$ = 1,375 $cm.^{-1}$
‡$\Omega_R$ = 1,638 $cm.^{-1}$

TABLE II

$O_2$-Dissociation (str. Hb)
$l_4(000) = 10.7\ s^{-1}$
$l_4(001) = 11.0\ s^{-1}$
$l_4(010) = 16.0\ s^{-1}$
$l_4(011) = 43.8\ s^{-1}$
$l_4(111) = 21.5\ s^{-1}$

CO-Dissociation (str. Hb)
$l_4(000) = 4.1 \times 10^{-3}\ s^{-1}$
$l_4(001) = 4.5 \times 10^{-3}\ s^{-1}$
$l_4(011) = 7.6 \times 10^{-3}\ s^{-1}$
$l_4(111) = 5.1 \times 10^{-3}\ s^{-1}$

CO-Association (str. Hb)
$l'_4(000) = 10.9 \times 10^6\ s^{-1}\ M^{-1}$
$l'_4(001) = 11.2 \times 10^6\ s^{-1}\ M^{-1}$
$l'_4(011) = 3.7 \times 10^6\ s^{-1}\ M^{-1}$
$l'_4(111) = 7.7 \times 10^6\ s^{-1}\ M^{-1}$

Dissociation and association rate constants ($K_4(ijk)$, $l_4(ijk)$, $l'_4(ijk)$ of the different titration states $C_{ijk}$ calculated by the fitting procedure.

by

$$HbL_4 \xrightarrow{l_4} HbL_3 + L$$

as the recombination process is blocked in the experiments of Noble and co-workers by fast irreversible binding of another ligand (for example CO binding after $O_2$-dissociation).

The reaction rate thus can be written as

$$\frac{\partial[HbL_4]}{\partial t} = -l_4[HbL_4]. \quad (10)$$

Association of a ligand (i.e., recombination of a ligand after dissociation by flash photolysis) is described by

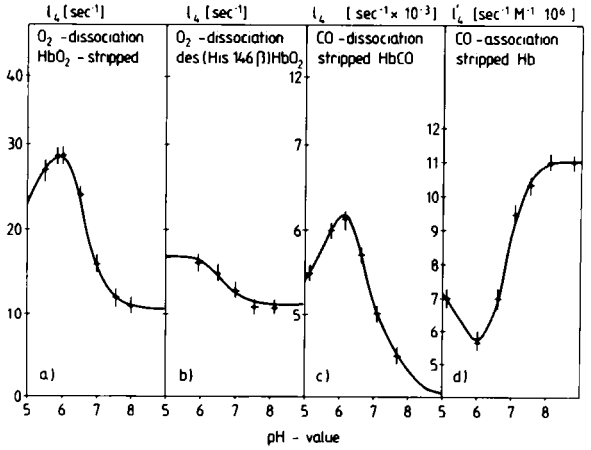


FIGURE 4 pH dependence of the fourth Hb-subunit $O_2$- and CO-dissociation (4*a*, *c*) and CO-association rate constants (4*d*); pH dependence of the fourth des(HisHC3β)Hb subunit $O_2$-dissociation rate constant (4*b*). (The data are obtained from Kwiatkowski and Noble (1982*a*) (Fig. 4*a*, *d*) and De Young et al. (1976), the full lines are calculated by the fitting procedure).

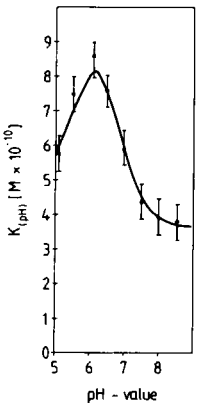


FIGURE 5 pH dependence of the fourth Hb subunit ligand affinity (the data are obtained from De Young et al. (1976), the full lines are calculated by the fitting procedure).

similar equations

$$HbL_3 + L \xrightarrow{l_4} HbL_4 \quad \frac{\partial[HbL_3]}{\partial t} = -l'_4[HbL_3][L]. \quad (11)$$

$[L]$ is the ligand concentration of the solution.

The solution of Eqs. 10 and 11 is given by

$$[HbL_4](t) = [HbL_4]_o e^{-l_4 t}$$
$$[HbL_3](t) = [HbL_3]_o e^{-l'_4 \nu' t}. \quad (12)$$

From the interpretation of the Raman data we now have to assume that dissociation- and association processes may be different for each molecular titration state. In this case Eq. 12 is a sum over different exponential functions

$$[HbL_4](t) = \sum_\nu [HbL_4]_{o_\nu} e^{-l_{4_\nu} t}$$

$$[HbL_3](t) = \nu = \sum_\nu [HbL_3]_{o_\nu} e^{-l'_{4_\nu}[L]t}$$

$$\nu = i, j, k. \quad (13)$$

Normalizing Eq. 13 to the total number of hemoglobin molecules, one obtains

$$\frac{[HbL_4](t)}{[HbL_4]_o} = \sum_\nu \frac{n_\nu}{N} e^{-l_{4_\nu} t} = e^{-l_{4_{eff}} t}$$
$$\frac{[HbL_3](t)}{[HbL_3]_o} = \sum_\nu \frac{n_\nu}{N} e^{-l'_{4_\nu}[L]t} = e^{-l'_{4_{eff}}[L]t}. \quad (14)$$

$n_\nu/N$ are the relative occupation numbers of the different titration states, and $l_{4_{eff}}$, $l'_{4_{eff}}$ represent effective rate constants measured from the first 60% of the reaction.

We have tried to fit Eq. 14 to the experimental data by using the titration model and its corresponding $pK$ values as obtained from the Raman data and treating the constants $l_4$, $l'_4$ as fitting parameters independent on pH. We have found that all the pH-dependent values of $l_{4_{eff}}$, $l'_{4_{eff}}$ could be fitted with one set $l_4$, $l'_4$, respectively.

The reaction constant curves calculated by the fitting

procedure are given by the full lines in Fig. 4 *a–c*. They are in excellent agreement with the experimental data. To test the quality of these results, we have tried to fit the data using different sets of *pK* values. In all cases the quality of the fits decreases. The calculated values $l_4$, $l'_4$ of the different titration states are summarized in Table II.

To identify the titrable groups affecting the pH dependence of ligand association/dissociation rate constants, Kwiatkowski and Noble have investigated des(his HC3$\beta$)Hb, because His HC3$\beta$ is a main candidate for the alkaline Bohr effect. Fig. 4 *b* shows that the pH dependence of $O_2$-dissociation is reduced in this system. Assuming tentatively that the value $pK = 7.8$ is related to His HC3$\beta$, we have fitted these data by using a titration model with only two *pK* values at $pK = 6.6$ and 5.8, and have found good agreement to the experimental data in Fig. 4. This result will be discussed in the next section.

In addition, Kwiatkowski and Noble (1982*a*) have measured the $O_2$-dissociation of des(His HC3$\beta$, Tyr HC2$\beta$)Hb also at low $Cl^-$ concentrations. In this case, pH dependence is nearly absent. One interesting aspect should be noted in this context. From the rate constants $l_{4_\nu}$, $l'_{4_\nu}$ one can calculate the activation energy difference between the different titration states by using a simple Arrhenius-model for the rate constants. For the $O_2$-dissociation one obtains a difference $\Delta G = 840$ cal/mol (3.5 KJ/mol) between the doubly protonated state $C_{011}$ and the deprotonated $C_{000}$. In comparison to this the protonation of the His HC3$\beta$ group (titration state $C_{001}$) causes a negligible small energy difference of 16 cal/mol (67 J/mol). This indicates a dominant role of the second protonation process due to $pK = 6.6$. The $O_2$-dissociation of des(His HC3$\beta$)Hb, however, can be related to an energy difference of 277 cal/mol (1.16 KJ/mol) between the different titration states of $pK = 6.6$ protonation. From this one can conclude that the group with $pK = 7.8$ has a drastic influence on the titration state $C_{011}$, although its direct contribution to the pH variation of $O_2$-dissociation is very small. This agrees well with our Raman data, which also exhibits a dominant role of the $pK = 6.6$ titration on the heme symmetry. Another important aspect of the kinetic measurements is obtained from Fig. 5, showing the pH dependence of the CO-binding equilibrium constant $K = l_4/l'_4$. This pH dependence of ligand affinity cannot be caused by *pK* shifts of the titrable groups with $pK = 5.8$, 6.6, and 7.8, since these *pK* values remain unchanged upon association or dissociation of the fourth ligand. We therefore propose tentatively the following model to explain the pH dependence of the fourth subunit ligand binding taking into account free energy conservation.

(*a*) The unliganded deoxy state is described by titrable states $C^U_{ijk}$ ($i, j, k = 0.1$ in the deprotonated, protonated state, respectively, where $U$ is the unliganded state) as defined in the section treating the theoretical background. (*b*) Upon ligation the oxy states $C^L_{ijk}$ ($L$ is the liganded state) with exception of titration states $C^L_{110}$ and $C^L_{010}$ switch into two different tertiary structures $L_1$ and $L_2$ in equilibrium with each other; denoted by $C^{L_1}_{ijk}$ and $C^{L_2}_{ijk}$ ($C^{L_3}_{ijk}$ in the acid region). The ligation proceses $C^U_{ijk} \rightarrow C^{L_1}_{ijk}$ and $C^{L_2}_{ijk}$ are thus described by different affinity constants $k^\mu = l^\mu_{4\nu}/l'_{4\nu}$ ($\mu = 1, 2, 3$), respectively.

These model assumptions are visualized by Fig. 6 showing the different energy levels of the liganded and unliganded states ($C_{011}$, $C_{101}$ are omitted because of their negligible contributions). On the left side the free energy levels of the deoxy state are shown reflecting the different titration states of Fig. 1. The liganded states on the right exhibit an energy splitting of the titration states $C^L_{000}$, $C^L_{100}$, $C^L_{011}$, and $C^L_{111}$, which are related to two different tertiary structures of the globular protein. The occupation numbers $n(C^u_{ijk})$, $n(C^L_{ijk})$ of the unliganded and liganded states can now simply be calculated using Eq. 9 and the mass action law for ligand binding between $C^u_{ijk}$ and $C^L_{ijk}$. The effective equilibrium constant $K_4$(pH) can be written

$$K(\mathrm{pH}) = \frac{\sum_{ijk} n(C^u_{ijk})\,[\mathrm{CO}]}{\sum_{\mu=1}^{3}\sum_{ijk} n(C^{L_\mu}_{ijk})} = \frac{[\mathrm{Hb(CO)_3}][\mathrm{CO}]}{[\mathrm{Hb(CO)_4}]}. \quad (15)$$

TABLE III

| | |
|---|---|
| $K^1_4 = 1.2 \times 10^{-9}$ M | $G^1_{K_4} = -12.3$ Kcal |
| $K^2_4 = 4.9 \times 10^{-10}$ M | $G^2_{K_4} = -12.82$ Kcal |
| $K^3_4 = 7.1 \times 10^{-10}$ M | $G^3_{K_4} = -12.6$ Kcal |

Equilibrium constants $K^\mu_4$($\mu = 1, 2, 3$) and the corresponding free energy differences for the CO binding of the fourth Hb subunit calculated by the fitting procedure.

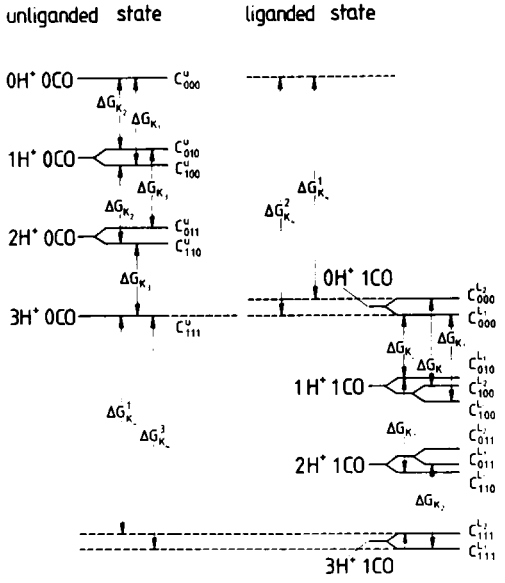


FIGURE 6 Free energy levels of the protonation states $C_{ijk}$ of the unliganded ($U$) and liganded state ($L$). The free energy differences $G^1_{K_4}$, $G^2_{K_4}$, $G^3_{K_4}$, are related to the equilibrium constants $K^1_4$, $K^2_4$, and $K^3_4$, respectively.

The thus defined effective equilibrium constant $K$ contains different contributions from equilibrium constants $K^{\mu}_{\nu} = l^{\mu}_{4,}/l^{\prime}_{4,}$ due to the different titration states. Therefore, we use the values of $K^{\mu}_{\nu}$ as free parameters in a fitting procedure. The results are visualized by the solid line in Fig. 5. The values for the free parameters $K^{\mu}_{\nu}$ and the corresponding free energy differences obtained from the fitting procedure are tabulated in Table III. From these values one can derive a free energy advantage of 0.53 Kcal/mol (2.3 KJ/mol) of CO ligandation in the alkaline region (pH 8) in comparison to the corresponding process at pH 6.0. The ligand binding in the acid region at pH 5.0 gains an energy of 0.3 Kcal/mol (1.3 KJ/mol).

We can summarize the main results of this section as follows: (*a*) From the measurements of the pH-induced DPR dispersion variation of oxyHb-Raman lines we obtain three titrable amino acid groups with $pK$ = 7.8, 6.6, and 5.8, which via apoprotein-heme interaction change the symmetry of the functional heme-group. The $pK$ values derived from Raman data agree well with those $pK$ values derived from kinetic measurements of the fourth subunit (CO-association/dissociation and $O_2$-dissociation pH dependence) by assuming that the kinetic processes are determined by contributions from different titration states. (*b*) The pH dependence of the CO-ligand affinity of the fourth hemoglobin subunit cannot be explained in terms of ligand-induced pH shifts of those titrable groups that influence the association and dissociation properties, since dissociation and association rate constants exhibit identical sets of $pK$ values. Therefore, a model is derived assuming that some titration states of the molecule split into two different tertiary states upon ligandation, which can be related to different equilibrium constants of ligand binding. This model enables us to explain the experimentally obtained pH dependence of ligand affinity.

## Tertiary "Induced Fit" Effects in the Hb-$\beta$ Subunits

Comparison of the kinetic data of ligand binding in Hb, des(His146$\beta$)Hb, and des(His HC3$\beta$, Tyr HC2$\beta$)Hb reflects a strong influence of Tyr HC3$\beta$ on the properties of the heme group. This can be interpreted from structural data in oxyHb, as reported by Shaanan (1983). He found that in the $R$ state, Tyr HC2$\beta$ forms an H-bond to Val FG5$\beta$ and in spite of this can exist in two conformations in equilibrium with each other It is reasonable to assume that protonation of nearby groups may shift this equilibrium. This is in accordance with our assumption of the energy splitting of the $C_{001}$ titration state.

Furthermore, one expects changes of heme-apoprotein interaction, since conformational changes of the Tyr-side chain via the hydrogen bond should induce changes in the FG-corner, which are transduced into the heme via central and peripheral coupling. In the case of oxyHb-BME constraints in the FG-corner by the BME-reagent block the influence of the H-bond. These findings are all in accordance to the pathway of Hb cooperativity, Perutz (1970).

The fact that the pH dependence of des(His HC3$\beta$)Hb is only determined by two $pK$ values (6.6, 5.8) cannot be interpreted uniquely. On the one hand, one can conclude, that the $pK$ = 7.8 may be related to His HC3$\beta$. This would agree well with the NMR measurements of Russu et al. (1980). Otherwise Perutz et al. (1985) have found His FG4 $\beta$ to exist in two different configurations with $pK$ = 6.0 and 7.6 in des(His HC3$\beta$)Hb, the equilibrium of which depends on ionic strength. At low $Cl^-$ concentrations the equilibrium is shifted to the configuration with $pK$ = 6.0. This also explains the missing $pK$ value of 7.6 in des(His HC3$\beta$) ligand dissociation.

The $pK$ value of 5.8 may be related to distal His E7 from the following experimental evidence: Ohm et al. (1979) have measured by NMR the titration of His E7 for oxymyoglobin obtaining a $pK$ value of 5.8. Asher et al. (1981) and Doster et al. (1980) report an influence of His E7 on the heme group of HbF and MbCO. In deoxyHb similar results are obtained from resonance Raman scattering (Schweitzer-Stenner et al., 1984*a*). El Naggar et al. (1985) have shown that below pH 6.5 a pH dependence of heme symmetry still exists in those systems lacking the saltbridge between His HC3$\beta$ and Asp HC1$\beta$. On the other hand Kwiatkowski and Noble have shown in another paper (1982*c*) that the acid part (pH <6.0) of the obtained pH influence on ligand binding is drastically reduced in des(Arg HC3$\alpha$)Hb. From this they conclude that the intramolecular saltbridge between Val NA1$\alpha$ and Arg HC3$\alpha$ also exists in the hemoglobin $R$ state. Since, however, both parts of the saltbridges protonate above pH 7.0 (Matthew 1979), the corresponding titration process influencing the stability of the saltbridge remains uncertain. Therefore, we assume that the $pK$ value of 5.8 can be related to His E7.

We summarize our results as follows: (*a*) The pH dependence of the hemoglobin $R$ state is mainly caused by the conformational change to Tyr HC2$\beta$, which exhibits a conformational change in oxyHb-$R$-state. This is caused by protonation of nearby histidines with $pK$ ~6.6. (*b*) Measuring and analyzation of the DPR-dispersion curves and the EPs of resonant Raman lines is a good completion to NMR-measurements, since information about correlations between tertiary structure variations of the protein and heme symmetry properties can thus be derived.

We gratefully acknowledge helpful discussions with Dr. Angela M. Gronenborn (MPI for Biochemie, Martinsried), who made available to us a preprint of the new paper of Perutz et al. (1985). Further, we would like to thank Dipl.-Chem. R. Düren for helpful discussions. We also thank Mr. G. Ankele for technical assistance, Mrs. C. Lamm for chemical assistance, Mrs. G. Waschwill for drawing the pictures, Mrs. B. Bödeker for typing the manuscripts and the "Gemeinschaftslaboratorium" of Drs. Schiwara, von Winterfeld, and Pfanzelt for making available to us freshly drawn blood.

## REFERENCES


Asher, S. A., M. L. Adams, and T. M. Schuster. 1981. Resonance Raman and absorption spectroscopic detection of distal histidine fluoride interactions in human methemoglobin fluoride and sperm whale metmyoglobin fluoride: measurements of distal histidine ionization constants. *Biochemistry.* 20:3339–3346.

Brunzel, U., W. Dreybrodt, and R. Schweitzer-Stenner. 1986. pH-dependent absorption in the B- and Q-bands of oxyhemoglobin and chemically modified oxyhemoglobin (BME) at low $Cl^-$-concentrations. *Biophys. J.* 49:1069–1076.

Deb, S. K., and M. L. Bansol. 1984. Calculation of error in depolarization ratio measurements due to finite collection angle in laser Raman spectroscopy. *Appl. Spectrosc.* 98:500–504.

DeYoung, A., R. R. Pennely, A. Tan-Wilson, and R. W. Noble. 1976. Kinetic studies on the binding affinity of human hemoglobin for the 4th carbon monoxide molecule $L_4$. *J. Biol. Chem.* 251:6692–6698.

Doster, W., D. Beece, S. F. Bowne, E. E. DiLorio, L. Eisenstein, H. Frauenfelder, L. Reinisch, E. Shyamsunder, H. Winterhalter, and K. T. Yue. 1982. Control and pH-dependence to heme proteins. *Biochemistry.* 21:4831–4839.

Englander, J. J., J. R. Rogero, and S. W. C. Englander. 1983. Identification of an allosterically sensitive unfolding unit in hemoglobin. *J. Mol. Biol.* 169:325–344.

Herzfeld, J., and H. E. Stanley. 1974. A general approach to cooperativity and its application to the oxygen equilibrium of hemoglobin and its effectors. *J. Mol. Biol.* 82:231–265.

Ikeda-Saito, M., H. Yamamoto, K. Imai, F. J. Kayne, and T. Yonetani. 1977. Studies on cobalt myoglobin and hemoglobin. *J. Biol. Chem.* 252:620–624.

Imai, K., and T. Yonetani. 1976. pH-dependence of the Adair constants of human hemoglobin. *J. Biol. Chem.* 250:2227–2232.

Imai, K. 1983. The Monod-Wyman-Changeux allosteric model describes haemoglobin oxygenation with only one adjustable parameter. *J. Mol. Biol.* 167:741–749.

Johnson, M. E., D. M. Scholler, B. M. Hoffman, and C. Ho. 1978. Tertiary structure variability within the quaternary states of hemoglobin: a spin label study. *Biochim. Biophys. Acta.* 535:193–205.

Kilmartin, J. V., J. J. Breen, J. C. K. Roberts, and C. Ho. 1973. Molecular mechanism of Bohr-effect. *Proc. Natl. Acad. Sci. USA.* 70:1246–1249.

Kilmartin, J. V., J. H. Fogg, and M. F. Perutz. 1980. Role of C-terminal histidine in the alkaline Bohr-effect of human hemoglobin. *Biochemistry.* 19:3189–3193.

Kwiatkowski, L., and R. W. Noble. 1982*a*. The effect of the 146$\beta$-histidine on the pH-dependence of the R-state of human hemoglobin. *In* Hemoglobin and Oxygen Binding. C. Ho, editor. Macmillan Press, Elsevier North-Holland. 403–407.

Kwiatkowski, L., and R. W. Noble. 1982*b*. The contribution of histidine (HC3) (146$\beta$) to the R-state Bohr-effect of human hemoglobin. *J. Biol. Chem.* 257:8891–8895.

Kwiatkowski, L., and R. W. Noble. 1982*c*. The effect of removal Arginine (141$\alpha$) on a pH-dependent kinetic property of the R-state of human hemoglobin A. *Fed. Proc.* 41:651.

Lindstrom, T. R., and C. Ho. 1973. Effects of anions and ligands on the tertiary structure around ligand binding site in human adult hemoglobin. *Biochemistry.* 12:134–139.

Loudon, R. 1973. The quantum theory of light. Clarendon Press, Oxford.

Matsukawa, S., Y. Itatani, K. Mawatari, Y. Shimokawa, and Y. Yoneyama. 1984. Quantitative evaluation for the role of $\beta$146 His and $\beta$147 His residues in the Bohr effect of human hemoglobin in the presence of 0.1 M chloride ion. *J. Biol. Chem.* 259:11479–11486.

Matthew, J. B., G. J. H. Hanania, and F. R. N. Gurd. 1974. Electrostatic effects in hemoglobin: hydrogen ion equilibrium in human deoxy- and oxyhemoglobin. A. *Biochemistry.* 18:1928–1963.

Mayer, A., and H. Eicher. 1984. Investigation of protein induced changes of the electronic structure of iron in heme proteins by HNMR spectroscopy. *J. Mol. Catal.* 23:151–161.

McDonald, M. I., and R. W. Noble. 1972. The effect on the rates of ligand replacement reactions of human adult and fetal hemoglobin and their subunit. *J. Biol. Chem.* 247:4282–4287.

Monod, J., J. Wynman, and J. P. C. Changeux. 1965. On the nature of allosteric transitions: a sensible model. *J. Mol. Biol.* 12:88–118.

El Naggar, S., W. Dreybrodt, and R. Schweitzer-Stenner. 1985. Haem-apoprotein interactions detected by resonance Raman scattering in Mb- and Hb-derivates lacking the saltbridge His146$\beta$-Asp94$\beta$. *Eur. Biophys. J.* 12:43–49.

Ohms, J. P., H. Hagenmaier, B. M. Hayes, and J. S. Cohen. 1979. Near-heme histidine residues of deoxy- and oxymyoglobins. *Biochemistry.* 18:1599–1602.

Ondrias, M. R., D. L. Rousseau, J. A. Shelnutt, and S. R. Simon. 1982. Quatenary-transformation-induced changes at the heme in deoxy hemoglobin. *Biochemistry.* 21:3420–3427.

Perutz, M. F. 1970*a*. Stereochemistry of cooperative effects in haemoglobin. *Nature (Lond.).* 228:726–734.

Perutz, M. F. 1970*b*. The Bohr-effect and combination with organic phosphates. *Nature (Lond.).* 228:734–739.

Perutz, M. F., J. E. Ladner, S. R. Simon, and C. Ho. 1974. Influence of globin structure on the state of the heme. I. Human deoxyhemoglobin. *Biochemistry.* 13:2163–2173.

Perutz, M. F., J. V. Kilmartin, K. Nishikura, J. H. Fogg, and P. J. G. Butler. 1980. Identification of residues contributing to the Bohr effect of human hemoglobin. *J. Mol. Biol.* 138:649–670.

Perutz, M. F., G. Fermi, and T.-b. Shih. 1984. Structure of deoxyhaemoglobin cowtown His HC3(146$\beta$) → Leu: origin of the alkaline Bohr effect and electrostatic interactions in hemoglobin. *Proc. Natl. Acad. Sci. USA.* 81:4781–4784.

Perutz, M. F., A. M. Gronenborn, G. M. Clore, J. H. Fogg, and T.-b. Shih. 1985. The $pK_a$-value of two histidine residues in human haemoglobin, the Bohr-effect, and the dipole moments of the $\alpha$ helices. *J. Mol. Biol.* 183:491–498.

Placzek, G. C. 1934. Rayleighstreuung und Ramaneffekt: In Marx (Ed.): Handbuch der Radiologie, Bd. 6. Akademische Verlagsgesellschaft Leipzig.

Rolema, H. S., H. M. Jansen, S. H. de Bruin, and G. van Os. 1975. The effect of potassium chloride of the Bohr effect of human hemoglobin. *J. Biol. Chem.* 250:1333–1339.

Roux-Fromy, M. 1982. On the hill plot of NMR-data for titration of protein residues. *Biophys. Struct. Mech.* 8:289–306.

Russu, I., N. T. Ho, and C. Ho. 1980. Role of $\beta$146 histidyl residues in the alkaline Bohr-effect of hemoglobin. *Biochemistry.* 19:1043–1052.

Russu, I., N. T. Ho, and C. Ho. 1982*a*. A proton nuclear magnetic resonance investigation of hystidyl residues in human normal adult hemoglobin. *Biochemistry.* 21:5031–5043.

Schweitzer-Stenner, R., W. Dreybrodt, and S. el Naggar. 1984*a*. Investigation of pH-induced symmetry distortions of the prosthetic group in deoxyhaemoglobin by resonance Raman scattering. *Biophys. Struct. Mech.* 10:241–256.

Schweitzer-Stenner, R., W. Dreybrodt, D. Wedekind, and S. el Naggar. 1984*b*. Investigation of pH-induced symmetry distortions of the prosthetic group in oxyhaemoglobin by resonance Raman scattering. *Eur. Biophys. J.* 11:61–76.

Schweitzer-Stenner, R., and W. Dreybrodt. 1984. Investigation of pH-induced symmetry distortions of the prosthetic group in oxyhaemoglobin by resonance Raman scattering. Proceedings of the IX-th International Conference on Raman spectroscopy, Tokyo. 748–749.

Schweitzer-Stenner, R., and W. Dreybrodt. 1985. Excitation profiles and

depolarization ratios of some prominent Raman lines in oxyhaemoglobin and ferrocytochrome c in the preresonant and resonant region of the Q-band. *J. Raman Spectrosc.* 16:111–123.

Shaanan, B. 1983. Structure of human oxyhaemoglobin at 2:1 Å resolution. *J. Mol. Biol.* 171:31–59.

Shih, T.-b., R. T. Jones, J. Bonaventura, C. Bonaventura, and R. G. Schneider. 1984. Involvement of HisHC3(146)$\beta$ in the Bohr-effect of human hemoglobin. Studies of native and N-ethylmaleimido-treated hemoglobin A and hemoglobin (Cowtown ($\beta$146His → Leu)). *J. Biol. Chem.* 259:967–974.

Simon, S. R., D. J. Arndt, and W. H. Königsberg. 1971. Structure and functional properties of chemically modified horse hemoglobin. *J. Mol. Biol.* 58:69–77.

Warshel, A., and R. Weiss. 1982. Strain and electrostatic contributions to cooperativity in hemoglobin, *In* Hemoglobin and Oxygen Binding. C. Ho, editor. Macmillan Press, London. 211–216.

Wedekind, D., S. el Naggar, R. Schweitzer-Stenner, and W. Dreybrodt. 1984. pH-induced changes of tertiary structure of oxyHbA detected by resonance Raman spectroscopy. *Proc. Int. Symp. Raman Spectros. Biol. Sci.* Osaka, Japan. 52.

Wedekind, D., R. Schweitzer-Stenner, and W. Dreybrodt. 1985. Heme-apoprotein interactions in the modified oxyhemoglobin-BME and in oxyhemoglobin at high $Cl^-$-concentration detected by resonance Raman scattering. *Biochem. Biophys. Acta.* 830:224–232.

El Yassin, D. I., and D. A. Fell. 1982. Comparison of the applicability of several allosteric models to the pH and 2,3 Bio (phospho) glycerate dependence of oxygen binding by human blood. *J. Mol. Biol.* 156:865–889.